IMA Journal of Applied Mathematics
doi: 10.1093/imamat/hxt006

Dead-time effects on the voltage spectrum of a PWM inverter

DAVID C. MOORE[†], MILIJANA ODAVIC[‡] AND STEPHEN M. COX[†]

[†]*School of Mathematical Sciences, University of Nottingham, University Park, Nottingham NG7 2RD, United Kingdom*
[‡]*Department of Electrical and Electronic Engineering, University of Nottingham, University Park, Nottingham NG7 2RD, United Kingdom*

An inverter converts a direct-current power supply to an alternating-current power supply. This conversion is achieved by switching the output between the inputs at high frequency. The resulting output voltage may be described by a high-frequency train of variable-width pulses. Pulse widths are slowly modulated so that this output waveform contains a prescribed low-frequency component, which may then be isolated by an appropriate filtering regime. Techniques for determining the full harmonic spectrum of input and output voltages and currents are well established, at least for an idealised mathematical model of the inverter. However, this model assumes that changes of inverter configuration can be effected instantaneously, which is not quite the case in practice. In fact, a small amount of *dead time* must be incorporated into switching regimes in order to avoid short circuits of the input. Although dead time is an important feature of real power conversion devices, its effects on output voltage spectra have not previously been fully determined (except by imposing rather restrictive approximations). This situation is remedied in the present paper, in which we present closed-form expressions for the coefficients of the harmonic spectrum, corroborated by simulations.

Keywords: power inverter, Fourier spectrum, harmonics, dead time

1. Introduction

The power inverter is an important technology for synthesising an alternating-current power supply from a direct-current source supply. The device achieves this power-supply conversion through semiconductor 'switches', which are rapidly opened and closed according to a prescribed *modulation strategy*, thereby changing the configuration of the device at high frequency. In the simple inverter design considered here, the output of the device is a sequence of square-wave pulses, the widths of which are slowly modulated at the frequency of the desired output. Such *pulse width modulation* (PWM) is used in a variety of electronic devices, including Class-D amplifiers (Berhout & Dooper, 2010; Cox *et al.*, 2011), fibre-optic communications equipment (Suh, 1987), and many others.

The slow modulation of the rapid switching in such devices has the unfortunate side-effect that the output voltages have complicated harmonic spectra. Knowledge of such spectra is of significant practical interest, particularly from the point of view of so-called *power quality*, and to inform the design of the filters needed to remove any unwanted frequency components. An idealised mathematical model is well established, and for a number of different PWM-based power-conversion devices the harmonic spectra of the output voltage signals are well documented (see, for example, Holmes & Lipo, 2003). Recovery of explicit expressions for the *input current* spectra is also feasible, as we have demonstrated elsewhere (Cox, 2009; Cox & Creagh, 2009).

Unfortunately, the present model assumes that the semiconductor 'switches' in power conversion devices operate instantaneously, which is not achievable in practice. To accommodate the nonzero switching durations of real semiconductor devices, switching times must be adjusted in order to avoid

a situation in which both switches conduct simultaneously and thus short-circuit the input. This adjustment is achieved through the addition of short periods of *dead time*, during which both switches are set to remain open, to allow time for the devices to change state without incident.

Previous investigations into the effects of dead time have largely been examinations of its effects on time-domain representations of the voltage and current waveforms and attempts to mitigate these through re-adjustment of the inverter (Leggate & Kerkman, 1997; Lin, 2002; Munoz & Lipo, 1999; Murai *et al.*, 1992; Oliviera *et al.*, 2007). That is not to say there have been no previous attempts to calculate the effects of dead time on the harmonic spectrum, but such ventures have employed additional approximations or unnecessarily restrictive assumptions about the switching times (Chierchie & Paolini, 2010; Wu *et al.*, 1999).

In this paper, we demonstrate that the effects of dead time can be incorporated into the harmonic spectrum of a power inverter *without* such additional approximations, and in a relatively straightforward manner. As one of the authors has argued elsewhere (Cox, 2009; Cox & Creagh, 2009), it is prudent to avoid the method typically adopted in the engineering literature (see Black, 1953) in favour of something less algebraically cumbersome. Other methods for determining spectra exist (see Pascual *et al.*, 2003; Song & Sarwate, 2003), but the technique espoused here seems to be the most straightforward.

There have been two notable prior attempts to determine the effects of switching dead time on the Fourier spectrum of the output voltages. First we mention Wu *et al.* (1999), who examine a two-phase (H-bridge) inverter with an inductive load. They use Black's method to determine the Fourier spectrum of the output in the presence of dead time. In the course of their analysis, an approximation is made, which amounts to the introduction of errors of the order of the (small) ratio of the power supply frequency to the switching frequency (ω_o/ω_s). The order of magnitude of the error due to this approximation is consistent with the discrepancies between their tabulated theoretical and simulated results. In a more recent work, Chierchie & Paolini (2010) derive a general formula for the Fourier spectrum coefficients, with and without dead time, but these formulas are written in terms of the switching times, so they give no immediate insight into the output voltage spectrum. One particular form of switching (so-called *natural sampling*) is then analysed in detail. Unfortunately, this analysis is limited to the case in which the ratio ω_s/ω_o is an integer and a further approximation is made to the equations for the switching times. Perhaps most unsatisfactory from an applications standpoint is the fact that the final result is left in terms of the switching times, so that no self-contained explicit expression for the Fourier coefficients is provided.

We begin our presentation of the effects of dead time on the output voltage spectrum of a PWM inverter, in Section 2, with a description of the inverter under consideration, before establishing the mathematical formulation of the problem in Section 3. The analysis proper can be found in Section 4. Corroborating numerical results are presented in Section 5, followed by a brief discussion and conclusion in Section 6.

2. Dead-time effects on a PWM inverter

Figure 1 shows the single-phase inverter considered in the present paper; for simplicity of notation, all voltages have been nondimensionalised so that the supply voltages take the values ± 1. This inverter represents the basic building block of most power converters. In what we shall refer to as the *ideal* model, one side of the load is held at zero volts while two switches connect the other side of the load alternately to the upper and lower supply rails (in practice, the switching is achieved using transistors). In parallel with these switches are diodes, which conduct current only in the direction shown; their significance will be explained in due course. The switching instants of the ideal output voltage are

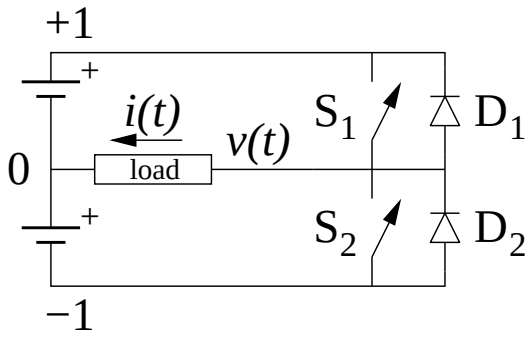

FIG. 1. Inverter design. Switches S_1 and S_2 operate alternately, at high frequency, to generate a quasi-periodic output voltage $v(t)$ whose low-frequency components are intended to deliver a prescribed alternating-current power supply.

denoted by A_m and B_m, and the corresponding output voltage pulse train is illustrated in Figure 2(a). However, in reality the semiconductor switches have significant turn-on and turn-off times, and so both switches may conduct around the switching instants, leading to a short-circuit of the input power supply, which is clearly unacceptable. One remedy is as follows: delay the 'on' signal for one switch (this delay is the *dead time*, T_d) to allow the other to completely turn off (to avoid a short-circuit of the input). In the mathematical model presented in Section 3, this approach of introducing delays will correspond to a parameter value $\delta = 1$. The output voltage associated with this case is depicted in Figure 2(b), together with that for the ideal case in Figure 2(a). Dead time can instead be introduced by advancing all turn-off times by $T_d/2$ and delaying all turn-on times by the same amount. This alternative approach will be associated with a parameter value $\delta = 0$. Figure 2(c) shows the corresponding output voltage waveform.

Clearly, when the upper switch (S_1) is closed, $v(t) = 1$, and with the lower switch (S_2) closed, $v(t) = -1$. During a dead-time episode (when both switches are open), the instantaneous output voltage $v(t)$ depends on the direction of the current through the load: this direction determines which of the diodes, D_1 or D_2, conducts. For example, suppose the current $i(t)$ through the load is negative. Then during the dead time around the switching *off* of S_2 and the switching *on* of S_1, diode D_1 conducts and D_2 blocks the current. For the same current polarity, during the dead time around S_2 switching *on* and S_1 *off*, D_1 again conducts and D_2 again blocks the current. The net result is an increase in the average voltage seen at the output across that switching cycle. By contrast, if the current $i(t)$ is *positive*, then there is a net decrease in the average voltage over the switching cycle. These dead-time effects modify the spectrum of the output voltage.

For completeness, we note that if the current is close to zero at the beginning of the dead time and decreases to zero during the dead time, then it will remain zero for the rest of the dead-time period, because the reverse-polarised diode blocks the current flow. This phenomenon can last for several switching periods, and causes additional distortion of the output voltage, beyond that modelled below. However, we anticipate that considering effects of this kind would result in only small changes to the spectrum recovered for typical ratios ω_o/ω_s.

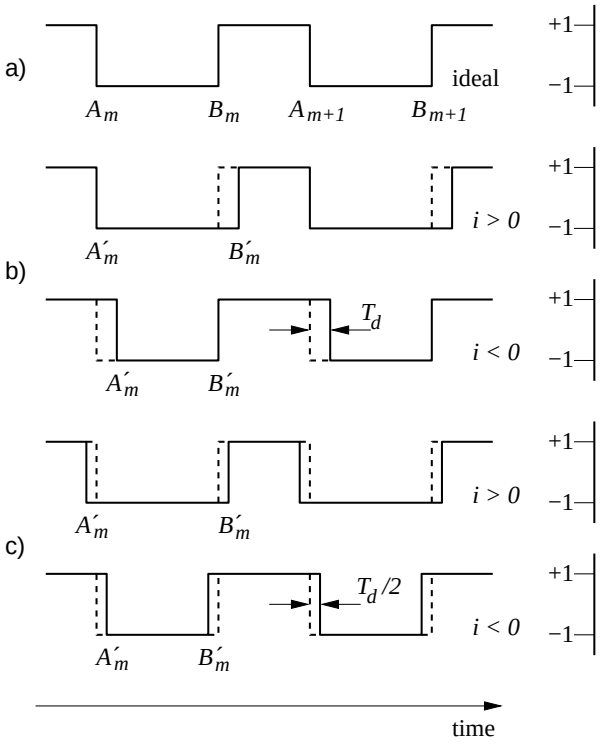

FIG. 2. Output voltage $v(t)$. (a) Ideal case, with no dead time. (b) Modified switching times, with dead time, in the case $\delta = 1$. (c) Modified switching times, with dead time, in the case $\delta = 0$. Note that the effect of dead time on the switching depends on the polarity of the output current $i(t)$.

3. Mathematical formulation

In this section, we develop a mathematical model for a single-leg power inverter. For clarity of exposition, we initially describe the model in the absence of any dead time. The modifications necessary to accommodate dead time are identified only once the fundamentals of the original 'ideal' model have been established. For further details of the simpler (zero-dead-time model) we also encourage the reader to consult Cox (2009).

The output voltage without any dead time, as pictured in Figure 3(a), is given by

$$v(t) = \begin{cases} +1 & \text{for } B_{m-1} < t < A_m, \\ -1 & \text{for } A_m < t < B_m. \end{cases} \tag{1}$$

The switching times A_m and B_m satisfy $mT_s < A_m < B_m < (m+1)T_s$, where T_s is the fundamental carrier period (see Figure 3). We shall refer to the interval $(mT_s, (m+1)T_s)$ as the mth switching period. If, for each t, t_1 and t_2, we let

$$\psi(t; t_1, t_2) = \begin{cases} 1 & \text{if } t_1 < t < t_2, \\ 0 & \text{otherwise,} \end{cases} \tag{2}$$

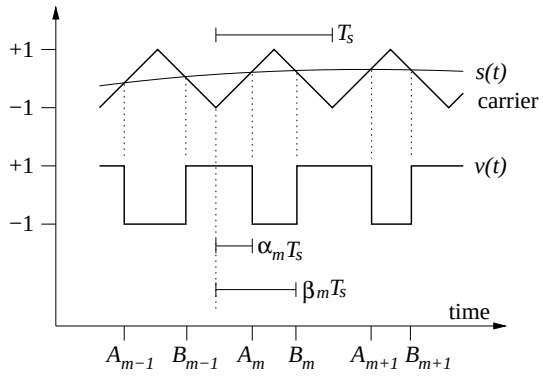

FIG. 3. PWM switching, illustrated for natural sampling of the reference signal $s(t)$. The voltage $v(t)$ takes the values $+1$ or -1 according to whether the value of the low-frequency reference wave $s(t)$ is greater than or less than the value of the high-frequency triangular carrier wave.

we may write

$$v(t) = 1 - 2\sum_{m=-\infty}^{\infty} \psi(t; A_m, B_m). \tag{3}$$

The switching times may be determined in a variety of ways, depending on the *sampling* method to be used. So-called *natural samping* is illustrated in Figure 3: the switching times are defined by the intersection of a low-frequency reference wave $s(t)$ (this is the desired alternating-current output voltage) with a high-frequency piecewise-linear carrier wave. Alternatively, the reference wave may be sampled at regular intervals, and this sampled value used to determine intersections with the carrier wave and hence the switching times. Both naturally and regularly sampled PWM are considered in this work. Furthermore, we treat two variants of regular sampling: if the reference signal is sampled only at the positive peaks of the triangular carrier waveform (or only at the negative peaks), this defines *symmetrical* regularly sampled PWM, whereas if the reference wave is sampled at *both* positive and negative peaks of the carrier, this defines *asymmetrical* regularly sampled PWM.

For any sampling method, the ideal switching times may be written in the form

$$A_m = (m + \alpha_m^\sigma)T_s, \qquad B_m = (m + \beta_m^\sigma)T_s, \tag{4}$$

where the superscript $\sigma = N$, *SR* or *AR* to denote, respectively, natural sampling, symmetrical regular sampling and asymmetrical regular sampling. The fractional switching times are given in terms of the reference signal by

$$\alpha_m^N = \tfrac{1}{4}(1 + s((m + \alpha_m^N)T_s)), \tag{5}$$
$$\beta_m^N = \tfrac{1}{4}(3 - s((m + \beta_m^N)T_s)), \tag{6}$$
$$\alpha_m^{SR} = \tfrac{1}{4}(1 + s(mT_s)), \tag{7}$$
$$\beta_m^{SR} = \tfrac{1}{4}(3 - s(mT_s)), \tag{8}$$
$$\alpha_m^{AR} = \tfrac{1}{4}(1 + s(mT_s)), \tag{9}$$
$$\beta_m^{AR} = \tfrac{1}{4}(3 - s((m + 1/2)T_s)). \tag{10}$$

Note that the switching times are determined explicitly for either form of regular sampling, but only implicitly for natural sampling. This crucial difference leads to slight differences in our treatment of the two sampling types. However, the corresponding modifications that must be made to the standard method (see Black, 1953) are considerably greater (Holmes & Lipo, 2003).

In this paper, results are calculated for a single-frequency reference wave,

$$s(t) = M\cos(\omega_o t), \tag{11}$$

where the amplitude M is often referred to as the *modulation depth*. With relatively minor modifications, but a considerable volume of additional algebra, the method used here can easily be extended to cater for multiple-frequency reference signals. In the absence of dead time, the output voltage spectrum which corresponds with (11) is well known (Holmes & Lipo, 2003). In applications, the output voltage switches between voltage levels at a frequency significantly in excess of that of the reference signal, so that $\omega_o T_s \ll 1$.

3.1 *Dead time*

In practice, as discussed above, the switching is subject to periods of dead time, during which the output voltage depends on the output current polarity. A full determination of the current polarity requires a full knowledge of the output voltage, and this interdependence leads to an apparently intractable problem.

However, an extremely good modelling assumption is to suppose that the current polarity changes sign precisely twice during each fundamental period of the reference signal. It is therefore reasonable to suppose that the current polarity is described by a step function $t \mapsto \Psi(t)$, as given by

$$\Psi(t) \equiv \operatorname{sgn}(\cos(\omega_o t - \Phi')) = \begin{cases} +1, & -\frac{1}{2}\pi + \Phi' < \omega_o t < \frac{1}{2}\pi + \Phi', \\ -1, & \frac{1}{2}\pi + \Phi' < \omega_o t < \frac{3}{2}\pi + \Phi', \end{cases} \tag{12}$$

with $\Psi(t) = \Psi(t + 2\pi/\omega_o)$ for all t. The determination of the phase angle Φ' requires a further modelling assumption. In the engineering literature, the assumption is that Φ' is the phase displacement between the fundamental components of the ideal output voltage and output current, which can readily be determined once the impedance of the output load is known. In any event, we shall take Φ' as known.

We now state the manner in which the switching times of the actual output voltage are determined. For regular sampling, these times (including dead time T_d) are prescribed by

$$A'_m = A_m + \tfrac{1}{2}(\delta - \Psi(mT_s))T_d, \qquad B'_m = B_m + \tfrac{1}{2}(\delta + \Psi(t_{B_m}))T_d, \tag{13}$$

where

$$t_{B_m} = \begin{cases} mT_s \text{ (symmetrical regular sampling, SR)}, \\ (m + 1/2)T_s \text{ (asymmetrical regular sampling, AR)}. \end{cases} \tag{14}$$

Here, the ideal switching times A_m and B_m are specified by (4), (7)–(10), and we recall that we have introduced the parameter δ taking the values 0 and 1 for the two dead-time implementations described above. For natural sampling, the actual switching times are given (implicitly) by

$$A'_m = \left(m + \tfrac{1}{4}(1 + s(A'_m))\right)T_s + \tfrac{1}{2}(\delta - \Psi(A'_m))T_d, \tag{15}$$

$$B'_m = \left(m + \tfrac{1}{4}(3 - s(B'_m))\right)T_s + \tfrac{1}{2}(\delta + \Psi(B'_m))T_d. \tag{16}$$

Before we turn to our analysis of the Fourier spectrum of the output voltage $v(t)$, we record two essential tools: we shall make repeated use of the Poisson re-summation formula (see, for example, Courant & Hilbert, 1989)

$$\sum_{m=-\infty}^{\infty} h(m) = \sum_{m=-\infty}^{\infty} \int_{-\infty}^{\infty} \mathrm{e}^{2\pi m \mathrm{i}\tau} h(\tau)\,\mathrm{d}\tau \tag{17}$$

and the Jacobi–Anger identity (Watson, 1944)

$$\mathrm{e}^{\mathrm{i}z\cos\theta} = \sum_{n=-\infty}^{\infty} \mathrm{i}^n \mathrm{J}_n(z)\mathrm{e}^{n\mathrm{i}\theta}. \tag{18}$$

4. Results

4.1 *Natural sampling*

In natural sampling regimes, switching times are known only implicitly, so it is remarkable that it is possible to recover a closed-form expression for (3). Progress is made by first applying the Poisson re-summation formula (17) to (3), to give

$$v(t) = 1 - 2\sum_{m=-\infty}^{\infty} \int_{-\infty}^{\infty} \mathrm{e}^{2\pi m \mathrm{i}\tau} \psi(t; A(\tau), B(\tau))\,\mathrm{d}\tau, \tag{19}$$

where $\tau \mapsto A(\tau)$ and $\tau \mapsto B(\tau)$ are continuous functions with the property that $A(m) = A'_m$ and $B(m) = B'_m$ for every integer m. In view of (15) and (16),

$$A(\tau) = \left(\tau + \tfrac{1}{4}(1 + M\cos(\omega_o A(\tau)))\right) T_s + \tfrac{1}{2}(\delta - \Psi(A(\tau)))T_d \equiv (\tau + \alpha(\tau))T_s, \tag{20}$$

$$B(\tau) = \left(\tau + \tfrac{1}{4}(3 - M\cos(\omega_o B(\tau)))\right) T_s + \tfrac{1}{2}(\delta + \Psi(B(\tau)))T_d \equiv (\tau + \beta(\tau))T_s. \tag{21}$$

The integrand in (19) is nonzero when

$$(\tau + \alpha(\tau))T_s < t < (\tau + \beta(\tau))T_s. \tag{22}$$

However, it turns out to be helpful to introduce functions $t \mapsto a(t)$ and $t \mapsto b(t)$ such that

$$a(t) = \alpha(\tau) \qquad \text{when } t = (\tau + \alpha(\tau))T_s, \tag{23}$$

$$b(t) = \beta(\tau) \qquad \text{when } t = (\tau + \beta(\tau))T_s. \tag{24}$$

Then, recalling (20) and (21), we see that $a(t)$ and $b(t)$ may be expressed explicitly in terms of t through

$$a(t) = \tfrac{1}{4}(1 + M\cos(\omega_o t)) + \tfrac{1}{2}(\delta - \Psi(t))T_d/T_s, \tag{25}$$

$$b(t) = \tfrac{1}{4}(3 - M\cos(\omega_o t)) + \tfrac{1}{2}(\delta + \Psi(t))T_d/T_s. \tag{26}$$

Using properties (23) and (24), we may equivalently write condition (22) as

$$\frac{t}{T_s} - b(t) < \tau < \frac{t}{T_s} - a(t). \tag{27}$$

The integrals in (19) are now readily calculated; thus

$$\begin{aligned} v(t) &= 1-2\sum_{m=-\infty}^{\infty}\int_{t/T_s-b(t)}^{t/T_s-a(t)} \mathrm{e}^{2\pi m\mathrm{i}\tau}\,\mathrm{d}\tau \\ &= 1-2(b(t)-a(t))-2\sum_{m=-\infty}^{\infty}{}' (2\pi m\mathrm{i})^{-1}\mathrm{e}^{2\pi m\mathrm{i}t/T_s}\left\{\mathrm{e}^{-2\pi m\mathrm{i}a(t)}-\mathrm{e}^{-2\pi m\mathrm{i}b(t)}\right\} \\ &= M\cos(\omega_o t)-\frac{2T_d}{T_s}\Psi(t)+\sum_{m=-\infty}^{\infty}{}' (\pi m\mathrm{i})^{-1}\mathrm{e}^{2m\mathrm{i}\pi t/T_s}\mathrm{e}^{-m\mathrm{i}\pi\delta T_d/T_s}\times \\ &\quad \left\{\mathrm{i}^m\mathrm{e}^{\mathrm{i}m\pi(\frac{1}{2}M\cos(\omega_o t)-\Psi(t)T_d/T_s)}-(-\mathrm{i})^m\mathrm{e}^{\mathrm{i}m\pi(-\frac{1}{2}M\cos(\omega_o t)+\Psi(t)T_d/T_s)}\right\}, \end{aligned} \tag{28}$$

where the notation $\sum'$ indicates that the term $m=0$ is omitted from the sum. We note that the only element of this formula that reflects the different implementations of dead time is the phase term involving δ. It is evident from (28) that the low-frequency contributions to the spectrum are due to

$$v(t)\sim M\cos(\omega_o t)-2\frac{T_d}{T_s}\Psi(t)+\cdots, \tag{29}$$

that is, precisely from the reference signal and a small-amplitude square wave with amplitude proportional to the dead-time ratio T_d/T_s.

To make further progress, we note that the exponentials in (28) which involve $\cos\omega_o t$ and $\Psi(t)$ are all $2\pi/\omega_o$-periodic, so may each be expressed in terms of a suitable Fourier series. In fact, each exponential may be written in the form

$$\mathrm{e}^{\mathrm{i}z\{\cos(\omega_o t)+\lambda\Psi(t)\}}\equiv\sum_{n=-\infty}^{\infty}S_n(z,\lambda)\mathrm{e}^{\mathrm{i}n\omega_o t}, \tag{30}$$

where the Fourier series coefficients $S_n(z,\lambda)$ may be obtained from

$$S_n(z,\lambda)=\frac{\omega_o}{2\pi}\int_0^{2\pi/\omega_o}\mathrm{e}^{\mathrm{i}z(\cos(\omega_o t)+\lambda\Psi(t))}\mathrm{e}^{-\mathrm{i}n\omega_o t}\,\mathrm{d}t. \tag{31}$$

Using the Jacobi–Anger relation (18) and the definition of Ψ from (12), we find

$$S_n(z,\lambda)=\cos(z\lambda)\mathrm{J}_n(z)\mathrm{i}^n+\sin(z\lambda)\mathrm{i}^n\sum_{\substack{p=-\infty\\ p\neq n}}^{\infty}[\pi(p-n)]^{-1}\mathrm{J}_p(z)\mathrm{e}^{\mathrm{i}(p-n)\Phi'}((-1)^{p-n}-1). \tag{32}$$

A Fourier series representation for $\Psi(t)$ is also readily obtained, and is given by

$$\Psi(t)=\frac{4}{\pi}\sum_{n=1,3,\ldots}^{\infty}\frac{(-1)^{\frac{1}{2}(n-1)}}{n}\cos(n(\omega_o t-\Phi')). \tag{33}$$

Finally, combining (28), (32) and (33), we find the output voltage to be

$$\begin{aligned} v(t) &= M\cos(\omega_o t)-\frac{8T_d}{T_s\pi}\sum_{n=1,3,\ldots}^{\infty}\frac{(-1)^{\frac{1}{2}(n-1)}}{n}\cos(n(\omega_o t-\Phi')) \\ &\quad +\sum_{m=-\infty}^{\infty}{}'\sum_{n=-\infty}^{\infty}\mathrm{i}^m(\pi m\mathrm{i})^{-1}\mathrm{e}^{-\mathrm{i}m\pi\delta T_d/T_s}\mathrm{e}^{\mathrm{i}\omega_{mn}t}\left\{S_n(\tfrac{1}{2}\pi mM,\lambda)-(-1)^m S_n(-\tfrac{1}{2}\pi mM,\lambda)\right\}, \end{aligned} \tag{34}$$

where

$$\lambda = -\frac{2T_d}{T_s M} \tag{35}$$

and the contributory frequencies in (34) are

$$\omega_{mn} = n\omega_o + m\frac{2\pi}{T_s} = n\omega_o + m\omega_s. \tag{36}$$

Consideration of the form of the term

$$S_n(\tfrac{1}{2}\pi mM, \lambda) - (-1)^m S_n(-\tfrac{1}{2}\pi mM, \lambda)$$

reveals that there are contributions to $v(t)$ with frequency ω_{mn} only when $m+n$ is odd. More explicitly, (34) may be written as

$$\begin{aligned} v(t) \;=\; & M\cos(\omega_o t) - \frac{8T_d}{T_s\pi}\sum_{n=1,3,\ldots}^{\infty}\frac{(-1)^{\frac{1}{2}(n-1)}}{n}\cos(n(\omega_o t - \Phi')) \\ & + \sum_{m=-\infty}^{\infty}{}'\sum_{n=-\infty}^{\infty} \mathrm{i}^{m+n}(\pi m\mathrm{i})^{-1}\mathrm{e}^{-\mathrm{i}m\pi\delta T_d/T_s}\mathrm{e}^{\mathrm{i}\omega_{mn}t}\times \\ & \left\{\cos(\pi mT_d/T_s)\mathrm{J}_n(\tfrac{1}{2}\pi mM)(1-(-1)^{m+n}) - \sin(\pi mT_d/T_s)\sum_{\substack{p=-\infty\\ p\neq n}}^{\infty}\frac{\mathrm{e}^{\mathrm{i}(p-n)\Phi'}}{\pi(p-n)}\mathrm{J}_p(\tfrac{1}{2}\pi mM)E_{mnp}\right\}, \end{aligned} \tag{37}$$

where

$$E_{mnp} = ((-1)^{p-n}-1)(1+(-1)^{m+p}). \tag{38}$$

It is apparent from (37) that the *fundamental* component of the actual voltage (i.e., the component with frequency ω_o) differs from the reference voltage $s(t)$ in both amplitude and phase, although these differences are small for all typical dead-time implementations (T_d/T_s on the order of a few percent). For a given value of the ratio T_d/T_s, the relative error in the fundamental is greater for smaller values of the modulation depth M.

4.2 *Asymmetrical regular sampling*

For regular sampling, the switching times are known explicitly, so the Fourier transform of the output voltage, $\hat{v}(\omega)$, may be obtained directly from (3). Thus, for asymmetrical sampling, from (3), (9), (10), (11), (13) and (14), it follows that, for $\omega \neq 0$,

$$\begin{aligned} \hat{v}(\omega) \;=\; & \int_{-\infty}^{\infty}\mathrm{e}^{-\mathrm{i}\omega t}v(t)\,\mathrm{d}t = -2\int_{-\infty}^{\infty}\mathrm{e}^{-\mathrm{i}\omega t}\sum_{m=-\infty}^{\infty}\psi(t;A_m,B_m)\,\mathrm{d}t \\ =\; & 2(-\mathrm{i}\omega)^{-1}\sum_{m=-\infty}^{\infty}\left(\mathrm{e}^{-\mathrm{i}\omega A_m} - \mathrm{e}^{-\mathrm{i}\omega B_m}\right) \\ =\; & 2(-\mathrm{i}\omega)^{-1}\sum_{m=-\infty}^{\infty}\mathrm{e}^{-\mathrm{i}m\omega T_s}\times \\ & \Big\{\mathrm{e}^{-\frac{1}{4}\mathrm{i}\omega T_s}\mathrm{e}^{\mathrm{i}\omega\left(-\frac{1}{4}T_sM\cos(m\omega_o T_s)+\frac{1}{2}T_d\Psi(mT_s)-\frac{1}{2}\delta T_d\right)} \\ & -\mathrm{e}^{-\frac{3}{4}i\omega T_s}\mathrm{e}^{i\omega\left(\frac{1}{4}T_sM\cos((m+\frac{1}{2})\omega_o T_s)-\frac{1}{2}T_d\Psi((m+\frac{1}{2})T_s)-\frac{1}{2}\delta T_d\right)}\Big\}. \end{aligned} \tag{39}$$

Poisson re-summing then gives

$$\hat{v}(\omega) = \frac{2}{-\mathrm{i}\omega} \sum_{m=-\infty}^{\infty} \int_{-\infty}^{\infty} \mathrm{e}^{2\pi m \mathrm{i}\tau} \mathrm{e}^{-\mathrm{i}\omega T_s \tau} \mathrm{e}^{-\frac{1}{2}\mathrm{i}\omega\delta T_d} Q(\tau)\,\mathrm{d}\tau, \tag{40}$$

where

$$\begin{aligned} Q(\tau) = {} & \mathrm{e}^{-\frac{1}{4}\mathrm{i}\omega T_s} \mathrm{e}^{\mathrm{i}\omega\left(-\frac{1}{4}T_s M\cos(\omega_o \tau T_s)+\frac{1}{2}T_d \Psi(\tau T_s)\right)} \\ & - \mathrm{e}^{-\frac{3}{4}\mathrm{i}\omega T_s} \mathrm{e}^{\mathrm{i}\omega\left(\frac{1}{4}T_s M\cos(\omega_o(\tau+\frac{1}{2})T_s)-\frac{1}{2}T_d \Psi((\tau+\frac{1}{2})T_s)\right)}. \end{aligned} \tag{41}$$

After substituting $t = \tau T_s$, we find, equivalently, that

$$\hat{v}(\omega) = \frac{2}{-\mathrm{i}\omega T_s} \sum_{m=-\infty}^{\infty} \int_{-\infty}^{\infty} \mathrm{e}^{2\pi \mathrm{i} m t/T_s} \mathrm{e}^{-\mathrm{i}\omega t} \mathrm{e}^{-\frac{1}{2}\mathrm{i}\omega\delta T_d} q(t)\,\mathrm{d}t, \tag{42}$$

where

$$\begin{aligned} q(t) = {} & \mathrm{e}^{-\frac{1}{4}\mathrm{i}\omega T_s} \mathrm{e}^{\mathrm{i}\omega\left(-\frac{1}{4}T_s M\cos(\omega_o t)+\frac{1}{2}T_d \Psi(t)\right)} \\ & - \mathrm{e}^{-\frac{3}{4}\mathrm{i}\omega T_s} \mathrm{e}^{\mathrm{i}\omega\left(\frac{1}{4}T_s M\cos(\omega_o(t+\frac{1}{2}T_s))-\frac{1}{2}T_d \Psi(t+\frac{1}{2}T_s)\right)}. \end{aligned} \tag{43}$$

The time-dependent exponentials in (43) may now be written as Fourier series, since they are each of the form in (30). Thus

$$q(t) = \mathrm{e}^{-\frac{1}{4}\mathrm{i}\omega T_s} \sum_{n=-\infty}^{\infty} S_n(-\tfrac{1}{4}\omega T_s M, \lambda) \mathrm{e}^{\mathrm{i}n\omega_o t} - \mathrm{e}^{-\frac{3}{4}\mathrm{i}\omega T_s} \sum_{n=-\infty}^{\infty} S_n(\tfrac{1}{4}\omega T_s M, \lambda) \mathrm{e}^{\mathrm{i}n\omega_o t} \mathrm{e}^{\mathrm{i}n\omega_o T_s/2}, \tag{44}$$

where λ is given in (35). Combining (42) and (44) then gives

$$\hat{v}(\omega) = \frac{2\mathrm{e}^{-\frac{1}{2}\mathrm{i}\omega\delta T_d}}{-\mathrm{i}\omega T_s} \sum_{m,n} \int_{-\infty}^{\infty} \mathrm{e}^{-i(\omega-\omega_{mn})t} \left\{ \mathrm{e}^{-\frac{1}{4}\mathrm{i}\omega T_s} S_n(-\tfrac{1}{4}\omega T_s M, \lambda) - \mathrm{e}^{-\frac{3}{4}\mathrm{i}\omega T_s} S_n(\tfrac{1}{4}\omega T_s M, \lambda) \mathrm{e}^{n\mathrm{i}\omega_o T_s/2} \right\} \mathrm{d}t. \tag{45}$$

Finally, by evaluating the integral in (45), we recover

$$v(t) = \sum_{m,n} V_{mn}^{AR} \mathrm{e}^{i\omega_{mn} t}, \tag{46}$$

where (provided $\omega_{mn} \neq 0$)

$$V_{mn}^{AR} = \frac{2\mathrm{e}^{-\frac{1}{2}\mathrm{i}\Omega_{mn}\delta T_d/T_s}}{-\mathrm{i}\Omega_{mn}} \left[\mathrm{e}^{-\frac{1}{4}i\Omega_{mn}} S_n(-\tfrac{1}{4}\Omega_{mn} M, \lambda) - \mathrm{e}^{-\frac{3}{4}i\Omega_{mn}} S_n(\tfrac{1}{4}\Omega_{mn} M, \lambda) \mathrm{e}^{in\pi\omega_o/\omega_s} \right] \tag{47}$$

and

$$\Omega_{mn} = T_s \omega_{mn} = n\omega_o T_s + 2\pi m. \tag{48}$$

More explicitly, (47) is given by (provided $\Omega_{mn} \neq 0$)

$$\begin{aligned} V_{mn}^{AR} = {} & \frac{2}{\mathrm{i}\Omega_{mn}} \mathrm{J}_n(\tfrac{1}{4}\Omega_{mn} M) \cos(\tfrac{1}{2}\Omega_{mn} T_d/T_s) \mathrm{e}^{-\frac{1}{4}\mathrm{i}\Omega_{mn}} \mathrm{e}^{-\frac{1}{2}\mathrm{i}\Omega_{mn}\delta T_d/T_s} \mathrm{i}^n ((-1)^m - (-1)^n) \\ & + \frac{2}{\mathrm{i}\Omega_{mn}} \sum_{\substack{p=-\infty \\ p\neq n}}^{\infty} \mathrm{J}_p(\tfrac{1}{4}\Omega_{mn} M) \sin(\tfrac{1}{2}\Omega_{mn} T_d/T_s) \frac{\mathrm{e}^{\mathrm{i}(p-n)\Phi'}}{\pi(p-n)} \mathrm{e}^{-\frac{1}{4}\mathrm{i}\Omega_{mn}} \mathrm{e}^{-\frac{1}{2}\mathrm{i}\Omega_{mn}\delta T_d/T_s} \mathrm{i}^n F_{mnp}, \end{aligned} \tag{49}$$

where

$$F_{mnp} = (1-(-1)^{p-n})((-1)^m + (-1)^p), \tag{50}$$

and $V_{mn}^{AR} = 0$ whenever $\Omega_{mn} = 0$.

It follows from (49) and (50) that $V_{mn}^{AR} = 0$ whenever $m+n$ is even. In particular, therefore, as for natural sampling, the even low-order harmonics (i.e. those for $m = 0$ and even n) are absent from the spectrum.

4.3 *Symmetrical regular sampling*

Following the procedure described in the previous subsection, but for symmetrical regular sampling, we find that (3), (7), (8), (11), (13) and (14) give

$$v(t) = \sum_{m,n} V_{mn}^{SR} \mathrm{e}^{\mathrm{i}\omega_{mn}t}, \tag{51}$$

where (provided $\Omega_{mn} \neq 0$) the Fourier coefficients are now

$$V_{mn}^{SR} = \frac{2}{-\mathrm{i}\Omega_{mn}} \mathrm{e}^{-\frac{1}{2}\mathrm{i}\Omega_{mn}\delta T_d/T_s} \left[\mathrm{e}^{-\frac{1}{4}\mathrm{i}\Omega_{mn}} S_n(-\tfrac{1}{4}\Omega_{mn}M, \lambda) - \mathrm{e}^{-\frac{3}{4}\mathrm{i}\Omega_{mn}} S_n(\tfrac{1}{4}\Omega_{mn}M, \lambda) \right]. \tag{52}$$

More explicitly, (52) is given by (whenever $\Omega_{mn} \neq 0$)

$$\begin{aligned} V_{mn}^{SR} &= \frac{2}{\mathrm{i}\Omega_{mn}} \mathrm{J}_n(\tfrac{1}{4}\Omega_{mn}M)\cos(\tfrac{1}{2}\Omega_{mn}T_d/T_s)\mathrm{e}^{-\frac{1}{4}\mathrm{i}\Omega_{mn}}\mathrm{e}^{-\frac{1}{2}\mathrm{i}\Omega_{mn}\delta T_d/T_s}\mathrm{i}^n(\mathrm{e}^{-\frac{1}{2}\mathrm{i}\Omega_{mn}} - (-1)^n) \\ &\quad + \frac{2}{\mathrm{i}\Omega_{mn}} \sum_{\substack{p=-\infty \\ p\neq n}}^{\infty} \mathrm{J}_p(\tfrac{1}{4}\Omega_{mn}M)\sin(\tfrac{1}{2}\Omega_{mn}T_d/T_s)\frac{\mathrm{e}^{\mathrm{i}(p-n)\Phi'}}{\pi(p-n)}\mathrm{e}^{-\frac{1}{4}\mathrm{i}\Omega_{mn}}\mathrm{e}^{-\frac{1}{2}\mathrm{i}\Omega_{mn}\delta T_d/T_s}\mathrm{i}^n G_{mnp}, \end{aligned} \tag{53}$$

where

$$G_{mnp} = (1-(-1)^{p-n})(\mathrm{e}^{-\frac{1}{2}i\Omega_{mn}} + (-1)^p); \tag{54}$$

and $V_{mn}^{SR} = 0$ whenever $\Omega_{mn} = 0$. No particular cancellation occurs in this case, so all harmonics are present.

5. Corroboration of analytical results

In this section, we compare our closed-form expressions for the harmonic spectrum of $v(t)$ with results from numerical 'simulations' of the inverter, obtained using Matlab.

The solid lines in Figures 4–6 represent the harmonic components obtained from our simulations. To give numerical results that are as clean as possible, we choose the ratio ω_s/ω_o to be an integer (although this restriction is not necessary for any of our analytical results). We choose a large number of equally spaced sample points over one period of the reference signal, then for each sample point we determine the corresponding output voltage, using the formulas in Section 3. Finally, we apply a Fast Fourier Transform (FFT) with 50000 points per switching period to this (sampled) output waveform. The numerical approximations to the Fourier coefficients thus obtained are plotted alongside those obtained through the analytical expressions derived in Section 4. Numerical and analytical results are marked, respectively, by solid and dashed lines. The results plotted are those corresponding to parameter values $\omega_s/\omega_o = 21$, $M = 0.8$, $\Phi' = 70.5 \times \pi/180$ and (whenever dead time is implemented) $T_d/T_s = 0.04$.

While the choice of an integer ratio ω_s/ω_o leads to particularly clean numerical results, it has the somewhat unfortunate consequence that harmonics can overlap: for example, in this case contributions to the frequency $3\omega_o$ can arise from $m = 0$, $n = 3$ or $m = 1$, $n = -18$, etc. Thus to determine the contribution at any given frequency, one must sum all such contributions (for an irrational ratio of frequencies, of course, no such issue arises).

Results shown are for $\delta = 1$; we have obtained similar agreement between numerical and analytical results for $\delta = 0$ dead time. Although, in applications, the dead time ratio T_d/T_s is typically around 0.01, we take $T_d/T_s = 0.04$ here so that the effects of dead time are sufficiently exaggerated to be visible in our plots. There is clearly excellent agreement between theory and simulation.

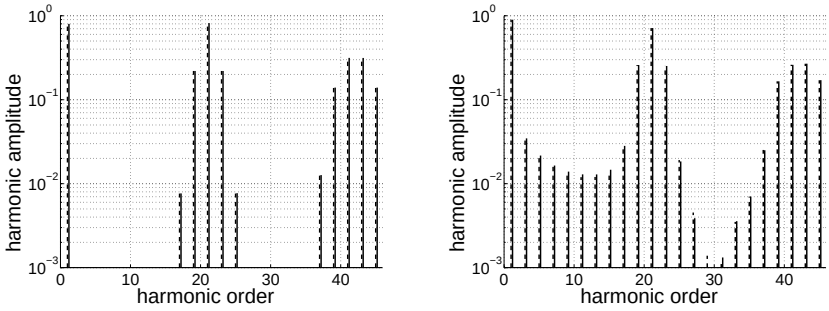

FIG. 4. Output voltage spectrum for natural sampling. Dashed lines show the theoretical spectrum; solid lines (slightly displaced for clarity) show results from simulation in Matlab. Left: $T_d = 0$. Right: $T_d/T_s = 0.04$ and $\delta = 1$. The frequency of a given contribution is 'harmonic order' $\times\, \omega_o$.

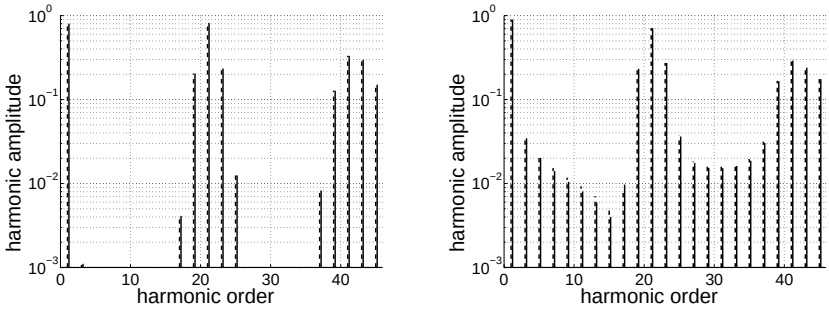

FIG. 5. Output voltage spectrum for asymmetrical regular sampling. Dashed lines show the theoretical spectrum; solid lines (slightly displaced for clarity) show results from simulation in Matlab. Left: $T_d = 0$. Right: $T_d/T_s = 0.04$ and $\delta = 1$. The frequency of a given contribution is 'harmonic order' $\times\, \omega_o$.

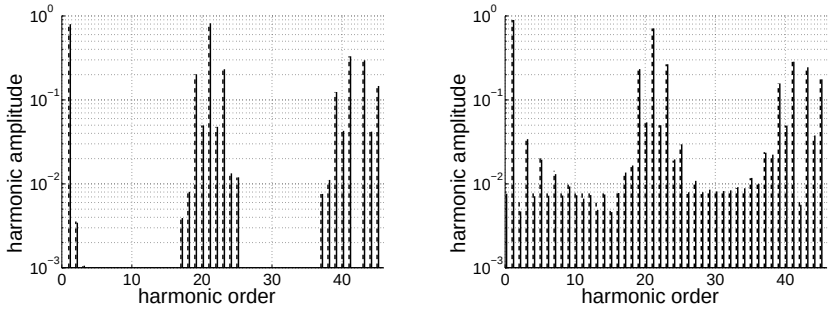

FIG. 6. Output voltage spectrum for symmetrical regular sampling. Dashed lines show the theoretical spectrum; solid lines (slightly displaced for clarity) show results from simulation in Matlab. Left: $T_d = 0$. Right: $T_d/T_s = 0.04$ and $\delta = 1$. The frequency of a given contribution is 'harmonic order' $\times\, \omega_o$.

6. Discussion and conclusions

This paper has presented closed-form expressions for the theoretical spectrum of the output voltage of a PWM inverter, allowing for two implementations of dead time, for the first time. Prior attempts to calculate the effects of dead time on this spectrum have relied on approximations or restrictions which are not necessary here. Our analysis reveals the influence of dead time upon the amplitudes of the low-order harmonics. For natural sampling, we find that the relationship between the dead-time ratio and the amplitudes of these components is linear. For regular sampling, the situation is similar, although the relationship is then only approximately linear, provided the ratio ω_o/ω_s is held fixed. For natural sampling and for asymmetrical regular sampling, we have identified those frequency components which are absent from the spectrum (these absences are independent of the form of the dead-time implementation).

We have corroborated our analytical results by means of Matlab simulations of the output voltage waveform. There is excellent agreement between theory and simulation for the two dead-time protocols discussed here, and for both natural and regular sampling.

One reason that dead-time effects have not previously been fully analysed lies in the tremendous algebraic complexity of the necessary calculations using the 'industry standard' method, due to Black (1953). We therefore emphasise that the method described here, although itself algebraically involved, is less cumbersome than Black's method, and does make feasible the dead-time calculation. Furthermore, it may readily be extended to allow for a multiple-frequency reference signal (cf. Odavic *et al.*, 2010), although, of course, the corresponding algebra would be significantly more involved. In a similar vein, we note that this method could be extended to more complicated power converter designs, for which the single-phase inverter presented here is the fundamental building block.

Finally, we note that in a practical implementation the spectrum may differ from the ideal case described here. For instance, with dead time the switching is determined by the *instantaneous*, rather than *sampled*, value of the current. It is therefore to be expected that occasional additional pulses may arise in the output voltage around the time at which the current changes polarity, modifying slightly the output voltage spectrum. While this effect is likely to be slight, its significance will increase as the ratio ω_o/ω_s increases; an analysis of this effect is beyond the scope of the present paper.

ACKNOWLEDGEMENTS

This work was supported by the Nuffield Foundation [URB/37857]. The authors would like to thank Stephen Creagh and Pericle Zanchetta for helpful conversations.

References

BERHOUT, M. & DOOPER, L. (2010) Class-D audio amplifiers in mobile applications, *IEEE Trans. Circuits and Systems I,* **57** 992–1002.

BLACK, H.S. (1953) *Modulation theory.* New York: Van Nostrand.

CHIERCHIE, F. & PAOLINI E.E. (2010) Analytical and numerical analysis of dead-time distortion in power inverters. In *Proceedings of the Argentine School of Micro–nanoelectronics, Technology and Applications*, pages 6–11.

COURANT, R. & HILBERT, D. (1989) *Methods of Mathematical Physics, Volume 1*. New York: Wiley-VCH.

COX, S.M. (2009) Voltage and current spectra for a single-phase voltage-source inverter, *IMA J. Appl. Math.,* **74** 782–805.

COX, S.M. & CREAGH, S.C. (2009) Voltage and current spectra for matrix power converters, *SIAM J. Appl. Math.,* **69** 1415–1437.

COX, S.M., TAN, M.T. & YU, J. (2011) A second-order class-D amplifier, *SIAM J. Appl. Math.,* **71** 270–287.

EVANS, P.D. & CLOSE, P.R. (1987) Harmonic distortion in PWM inverter output waveforms, *Electric Power Applications, IEE Proceedings B,* **134** 224–232.

HOLMES, D.G & LIPO, T.A. (2003) *Pulse width modulation for power converters.* New York: Wiley-VCH.

LEGGATE, D. & KERKMAN, R.J. (1997) Pulse-based dead-time compensator for PWM voltage inverters, *IEEE Trans. Industr. Electron.,* **44** 191–197.

MUNOZ, A.R. & LIPO, T.A. (1999) On-line dead-time compensation technique for open-loop PWM-VSI drives, *IEEE Trans. Power Electron.,* **14** 683–689.

LIN, J.L. (2002) A new approach of dead-time compensation for PWM voltage inverters, *IEEE Trans. Circuits and Systems I,* **49** 476–483.

MURAI, Y., RIYANTO, A., NAKAMURA, H. & MATSUI, K. (1992) PWM strategy for high frequency carrier inverters eliminating current clamps during switching dead-time, in *Proc. IEEE Ind. Appl. Soc. Annu. Meeting,* 317–322.

ODAVIC, M., SUMNER, M., ZANCHETTA, P. & CLARE, J.C. (2010) A theoretical analysis of the harmonic content of PWM waveforms for multiple-frequency modulators, *IEEE Trans. Power Electron.,* **25** 131–141.

OLIVEIRA, A.C., JACOBINA, C.B. & LIMA, A.M.N. (2007) Improved dead-time compensation for sinusoidal PWM inverters operating at high switching frequencies, *IEEE Trans. Industr. Electron.*, **54** 2295–2304.

PASCUAL, C., SONG, Z., KREIN, P.T., SARWATE, D.V., MIDYA, P. & ROECKNER, W.J. (2003) High-fidelity PWM inverter for digital audio amplification: spectral analysis, real-time DSP implementation, and results, *IEEE Trans. Power Electronics,* **18** 473–485.

SONG, Z. & SARWATE, D.V. (2003) The frequency spectrum of pulse width modulated signals, *Signal Processing,* **83** 2227–2258.

SUH, S. (1987) Pulse width modulation for analog fiber-optic communications, *J. Lightwave Technology,* **5** 102–112.

WATSON, G.N. (1944) *A treatise on the theory of Bessel functions.* Cambridge, UK: Cambridge University Press.

WU, C.M., LAU, W.-H. & CHUNG, H.S.-H (1999) Analytical technique for calculating the output harmonics of an H-bridge inverter with dead time, *IEEE Trans. Circuits and Systems I,* **46** 617–627.